

Tensorial slip of superhydrophobic channels

Sebastian Schmieschek,^{1,2} Aleksey V. Belyaev,^{3,4} Jens Harting,^{2,1} and Olga I. Vinogradova^{3,4,5}

¹*Institute for Computational Physics, University of Stuttgart, Pfaffenwaldring 27, DE-70569 Stuttgart, Germany*

²*Department of Applied Physics, Eindhoven University of Technology, P.O. Box 513, NL-5600 MB Eindhoven, The Netherlands*

³*Department of Physics, M.V. Lomonosov Moscow State University, 119991 Moscow, Russia*

⁴*A.N. Frumkin Institute of Physical Chemistry and Electrochemistry, Russian Academy of Sciences, 31 Leninsky Prospect, 119991 Moscow, Russia*

⁵*DWI, RWTH Aachen, Forckenbeckstrasse 50, DE-52056 Aachen, Germany*

(Received 2 September 2011; revised manuscript received 18 November 2011; published 27 January 2012)

We describe a generalization of the tensorial slip boundary condition, originally justified for a thick (compared to texture period) channel, to any channel thickness. The eigenvalues of the effective slip-length tensor, however, in general case become dependent on the gap and cannot be viewed as a local property of the surface, being a global characteristic of the channel. To illustrate the use of the tensor formalism we develop a semianalytical theory of an effective slip in a parallel-plate channel with one superhydrophobic striped and one hydrophilic surface. Our approach is valid for any local slip at the gas sectors and an arbitrary distance between the plates, ranging from a thick to a thin channel. We then present results of lattice Boltzmann simulations to validate the analysis. Our results may be useful for extracting effective slip tensors from global measurements, such as the permeability of a channel, in experiments or simulations.

DOI: [10.1103/PhysRevE.85.016324](https://doi.org/10.1103/PhysRevE.85.016324)

PACS number(s): 47.61.-k, 47.11.-j, 83.50.Rp

I. INTRODUCTION

With recent advances in microfluidics [1,2], renewed interest has emerged in quantifying the effects of surface heterogeneities with different local hydrophobicity (characterized by a local scalar slip [3,4]), on fluid motion. In this situation it is advantageous to construct the effective slip boundary condition, which is applied at the hypothetical smooth homogeneously slipping surface, and mimics the actual one along the true heterogeneous surface [5,6]. Such an effective condition fully characterizes the flow at the real surface and can be used to solve complex hydrodynamic problems without tedious calculations. Well-known examples of such a heterogeneous system include superhydrophobic (SH) Cassie surfaces, where trapped gas is stabilized with a rough wall texture, leading to a number of “super” properties, such as extreme nonwettability and low hysteresis [7]. For these surfaces effective slip lengths are often very large [8–11] compared with a smooth hydrophobic coating [12–17], which can greatly reduce the viscous drag and impact transport phenomena in microchannels [5].

The concept of effective slip was mostly exploited for *thick* (compared to the texture characteristic length, L) channels [1,18], where for an anisotropic texture it was shown to depend on the direction of the flow and is a tensor [19], $\mathbf{b}_{\text{eff}} \equiv \{b_{ij}^{\text{eff}}\}$, represented by a symmetric, positive definite 2×2 matrix

$$\mathbf{b}_{\text{eff}} = \mathbf{S}_{\Theta} \begin{pmatrix} b_{\text{eff}}^{\parallel} & 0 \\ 0 & b_{\text{eff}}^{\perp} \end{pmatrix} \mathbf{S}_{-\Theta}, \quad (1)$$

diagonalized by a rotation with angle Θ ,

$$\mathbf{S}_{\Theta} = \begin{pmatrix} \cos \Theta & \sin \Theta \\ -\sin \Theta & \cos \Theta \end{pmatrix}. \quad (2)$$

For all anisotropic surfaces its eigenvalues $b_{\text{eff}}^{\parallel}$ and b_{eff}^{\perp} correspond to the fastest (greatest forward slip) and slowest (least

forward slip) orthogonal directions [19]. In the general case of any direction Θ , this means that the flow past such surfaces becomes misaligned with the driving force. This tensorial slip approach, based on a consideration of a “macroscale” fluid motion instead of solving hydrodynamic equations at the scale of the individual pattern, was supported by statistical diffusion arguments [19], and was recently justified for the case of Stokes flow over a broad class of periodic surfaces [6]. Note that an effective slip in a thick channel situation is a characteristic of a heterogeneous interface solely (being expressed through its parameters, such as local slip lengths, fractions of phases, and a texture period) [5,20].

It was, however, recently recognized and justified by using the theory of heterogeneous porous materials [21] that a similar concept of effective slip can also be exploited for a flow conducted in a *thin* channel with two confining surfaces separated by a distance $H \ll L$. In such a situation a natural definition of the effective slip length could be based on a permeability of a hypothetical uniform channel with the same flow rate. An effective tensorial slip is then determined by flow at the scale of the channel width, and depends on H [21]. This points to the fact that an effective boundary condition reflects not just parameters of the liquid-solid interface, but also depends on the flow configuration [5].

The power of the effective slip approach and the superlubrication potential of SH surfaces were already illustrated by discussing several applications. In particular, it has been shown that optimized SH textures may be successfully used in passive microfluidic mixing [5,22] and for a reduction of a hydrodynamic drag force [23,24], and that the effective slip formalism represents a useful tool to quantify properties of SH surfaces in thick and thin channels. In many situations, however, the dramatic changes in flow happen when the two length scales H and L are of the same order. In this work we generalize the definition of the effective slip-length tensor Eq. (1) to an *arbitrary* channel thickness and validate this approach by means of lattice Boltzmann (LB) simulations.

The structure of this manuscript is as follows. In Sec. II we describe our model and formulate governing equations. In Sec. III we analyze a tensorial permeability of the parallel-plate channel with one (anisotropic) SH and one hydrophilic surface and give some general arguments showing that the tensorial relation, Eq. (1), should be valid at arbitrary H/L . Section IV contains semianalytical results for a striped SH surface, and in Sec. V we describe our LB simulation approach. In Sec. VI simulation results are presented to validate the predictions of the tensorial theory and to test our analytical results for the asymptotic limits of thick and thin channels.

II. MODEL AND GOVERNING EQUATIONS

The basic assumptions of our theoretical model are as follows. We consider a channel consisting of two parallel walls located at $y = 0$ and $y = H$ and unbounded in the x and z directions as sketched in Fig. 1. The upper plate represents a no-slip hydrophilic surface, and the lower plate is a SH surface. The origin of coordinates is placed in the plane of a liquid-gas interface at the center of the gas sector. The x axis is defined along the pressure gradient. This (SH vs hydrophilic) geometry of configuration is relevant for various setups, where the alignment of opposite textures is inconvenient or difficult. In addition, the advantage of such a geometry is that it allows one to avoid the gas bridging and long-range attractive capillary forces [25], which appear when we deal with interactions of two hydrophobic solids [26,27].

As in previous publications [20,23,28], we model the SH plate as a flat interface with no meniscus curvature,

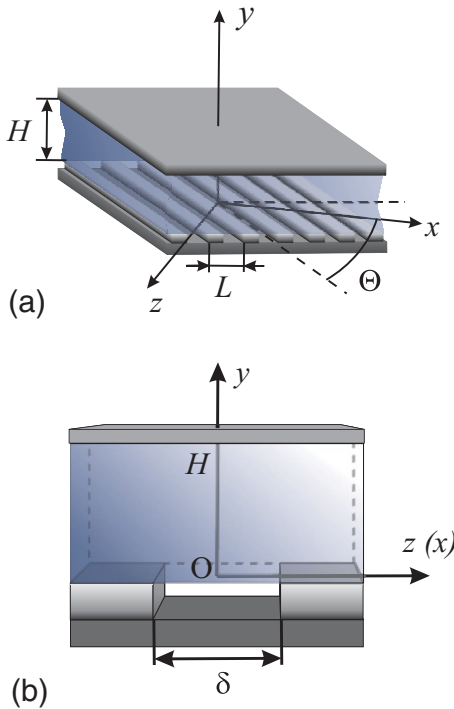


FIG. 1. (Color online) Sketch of the SH stripes: (a) $\Theta = \pi/2$ corresponds to transverse stripes, whereas $\Theta = 0$ corresponds to longitudinal stripes; (b) the situation in (a) is approximated by a periodic cell of size L , with equivalent flow boundary conditions on the gas-liquid and solid-liquid interfaces.

so that the SH surface appears as perfectly smooth with a pattern of boundary conditions. The latter are taken as no-slip ($b_1 = 0$) over solid/liquid areas and as partial slip ($b_2 = b$) over gas/liquid regions. We denote as δ a typical length scale of gas/liquid areas. The fraction of the solid/liquid areas is denoted $\phi_1 = (L - \delta)/L$, and that of the gas/liquid areas is denoted $\phi_2 = 1 - \phi_1 = \delta/L$. In this idealization, by assuming a flat interface, we neglect an additional mechanism for a dissipation connected with the meniscus curvature [14,29,30].

The flow is governed by the Stokes equations

$$\eta \nabla^2 \mathbf{u} = \nabla p, \quad (3)$$

$$\nabla \cdot \mathbf{u} = 0, \quad (4)$$

where \mathbf{u} is the velocity vector, and the average pressure gradient is always aligned with the x -axis direction:

$$\langle \nabla p \rangle = (-\sigma, 0, 0). \quad (5)$$

The local slip boundary conditions at the walls are defined as

$$\mathbf{u}(x, 0, z) = b(x, z) \cdot \frac{\partial \mathbf{u}}{\partial y}(x, 0, z), \quad \hat{\mathbf{y}} \cdot \mathbf{u}(x, 0, z) = 0, \quad (6)$$

$$\mathbf{u}(x, H, z) = 0, \quad \hat{\mathbf{y}} \cdot \mathbf{u}(x, H, z) = 0. \quad (7)$$

Here the local slip length $b(x, z)$ at the SH surface is generally the function of both lateral coordinates.

We intend to evaluate the effective slip length b_{eff} at the SH surface, which is as usual defined as

$$b_{\text{eff}} = \frac{\langle u_s \rangle}{\left(\left\langle \frac{\partial u}{\partial y} \right\rangle_s \right)}, \quad (8)$$

where $\langle \dots \rangle$ means the average value in the plane xOz .

III. GENERAL CONSIDERATION

In this section, we evaluate the pressure-driven flow in the parallel-plate channel with one anisotropic SH and one hydrophilic surface and investigate the consequences of anisotropy. For an anisotropic texture, there are several possible ways to define effective slip lengths. A natural approach is to define a slip-length tensor via

$$k^{\parallel, \perp} = \frac{H^3}{12} \left(1 + \frac{3b_{\text{eff}}^{\parallel, \perp}}{H + b_{\text{eff}}^{\parallel, \perp}} \right) \quad (9)$$

by analogy with a hypothetical uniform channel. Such a definition was earlier justified for thin SH channels, by using the lubrication limit [21]. Below we argue that the same result is obtained for a channel of an arbitrary thickness with a tensorial generalization of the Navier boundary condition, where \mathbf{b}_{eff} is a global measure of the effective slippage of the channel.

For a mathematical justification of the above statement we first rewrite Eqs. (3) and (5) as

$$\eta \nabla^2 \langle \mathbf{U} \rangle = \langle \nabla p \rangle, \quad \langle \nabla p \rangle = -\sigma \hat{\mathbf{x}}, \quad (10)$$

where $\langle \mathbf{U} \rangle$ is the depth-averaged velocity. The two boundary conditions that apply at the channel walls can then be written as follows: $\langle \mathbf{U} \rangle = 0$ at the upper surface, and uniform tensorial slip,

$$\langle \mathbf{U} \rangle = \mathbf{b}_{\text{eff}} \cdot \langle \partial_y \mathbf{U} \rangle, \quad (11)$$

at the lower surface, with \mathbf{b}_{eff} defined according to Eqs. (1) and (2). The solution for the depth-averaged velocity is then given by [5]

$$\langle U_x \rangle = -\frac{\sigma y^2}{2\eta} + \frac{\sigma H y}{2\eta} + \frac{\sigma H^2}{2\eta} C_x \left(1 - \frac{y}{H}\right), \quad (12)$$

$$\langle U_z \rangle = \frac{\sigma H^2}{2\eta} C_z \left(1 - \frac{y}{H}\right), \quad (13)$$

with

$$C_x = \frac{H b_{\text{eff}}^{\parallel} \cos^2 \Theta + H b_{\text{eff}}^{\perp} \sin^2 \Theta + b_{\text{eff}}^{\parallel} b_{\text{eff}}^{\perp}}{(H + b_{\text{eff}}^{\parallel})(H + b_{\text{eff}}^{\perp})},$$

$$C_z = \frac{H(b_{\text{eff}}^{\parallel} - b_{\text{eff}}^{\perp}) \sin \Theta \cos \Theta}{(H + b_{\text{eff}}^{\parallel})(H + b_{\text{eff}}^{\perp})}.$$

In linear response, the averaged flow rate, $\langle \mathbf{Q} \rangle$, is proportional to $\langle \nabla p \rangle$ via the permeability tensor, \mathbf{k} :

$$\langle \mathbf{Q} \rangle = -\frac{1}{\eta} \mathbf{k} \cdot \langle \nabla p \rangle. \quad (14)$$

Integrating the velocity profile across the channel we obtain

$$\langle \mathbf{Q} \rangle = \int_0^H \langle \mathbf{U}(y) \rangle dy, \quad (15)$$

with the components

$$\langle Q \rangle_x = \frac{\sigma H^3}{\eta} \frac{1}{12} [1 + 3C_x], \quad \langle Q \rangle_z = \frac{\sigma H^3}{\eta} \frac{1}{4} C_z. \quad (16)$$

The latter may be rewritten as

$$\langle Q \rangle_x = \frac{\sigma}{\eta} (k^{\parallel} \cos^2 \Theta + k^{\perp} \sin^2 \Theta), \quad (17)$$

$$\langle Q \rangle_z = \frac{\sigma}{\eta} (k^{\parallel} - k^{\perp}) \sin \Theta \cos \Theta, \quad (18)$$

provided the two tensors, \mathbf{k} and \mathbf{b}_{eff} , are coaxial and the rigorous relationship between their eigenvalues is given by Eq. (9). This unambiguously indicates that the two definitions of the slip length are equivalent. It also becomes apparent that Eq. (9) implies that $b_{\text{eff}}^{\parallel, \perp}$ generally depends on the separation H .

Note some similarity to a prior work [21,31]. The current consideration, however, is valid for arbitrary H/L and b/L , including the limit of thick channels, where \mathbf{b}_{eff} becomes a local property of the surface on scales much larger than the texture characteristic length.

Consider now a situation where the “fast” axis of greatest forward slip of anisotropic texture is inclined at an angle Θ to the pressure gradient. This problem can be solved explicitly as follows. The downstream effective permeability of the channel can be expressed in terms of the effective downstream slip length as

$$k_{\text{eff}}^{(x)} = \frac{H^3}{12} \left(1 + \frac{3b_{\text{eff}}^{(x)}}{H + b_{\text{eff}}^{(x)}}\right). \quad (19)$$

Following [19], it can also be obtained from the permeability tensor:

$$k_{\text{eff}}^{(x)} = \frac{k^{\parallel} k^{\perp}}{k^{\parallel} \sin^2 \Theta + k^{\perp} \cos^2 \Theta}. \quad (20)$$

By substituting Eq. (9) into Eq. (20) and after subtracting the latter from Eq. (19) we express an effective downstream slip length in the form

$$b_{\text{eff}}^{(x)} = \frac{b_{\text{eff}}^{\perp} H + 4b_{\text{eff}}^{\parallel} b_{\text{eff}}^{\perp} + (b_{\text{eff}}^{\parallel} - b_{\text{eff}}^{\perp}) H \cos^2 \Theta}{H + 4b_{\text{eff}}^{\parallel} - 4(b_{\text{eff}}^{\parallel} - b_{\text{eff}}^{\perp}) \cos^2 \Theta}. \quad (21)$$

Note that in the general case $b_{\text{eff}}^{(x)}$ depends on H and $b_{\text{eff}}^{\parallel, \perp}(H)$. For this reason, $b_{\text{eff}}^{(x)}$ cannot be viewed as a *local* property of the SH surface, except as in the thick channel limit. Instead, it is generally the effective slip length of the SH channel and thus its *global* characteristic.

Finally, we emphasize the generality of Eqs. (20) and (21), which follow only from the symmetry of the effective permeability and slip-length tensors for linear response. Similar formulas have been obtained before in a few particular calculations Refs. [31,32], but the present derivation is valid regardless of the thickness of the channel and is independent of the details of the textured surface. There could be arbitrary patterns of local slip lengths, and the latter could itself be a spatially varying tensor, reflecting surface anisotropy at a smaller (possibly atomic) scale.

IV. THEORY FOR STRIPED PATTERNS

To illustrate the general theory, in this section we focus on flat patterned SH surfaces consisting of periodic stripes, where the local (scalar) slip length b varies only in one direction. The problem of flow past striped SH surfaces has previously been studied in the context of a reduction of pressure-driven forward flow in thick [28,33,34] and thin [21] channels, and it is directly relevant for mixing [5,22], and generation of a tensorial electro-osmotic flow [5,35,36]. Here we elaborate on a previously published ansatz [5] and present the theory for an arbitrary gap, which in the asymptotic limits describes situations of thin and thick channels. The mathematical analysis we use here is similar to a technique exploited in Ref. [34] for a thick channel configuration. The crucial difference with Ref. [34], however, is that we consider an arbitrary gap, which means that the effective slip is a function of the channel thickness as discussed above.

For transverse stripes, we have $\mathbf{u} = (u(x, y), v(x, y), 0)$, $u(x, 0) = b(x)u_y(x, 0)$, and $v(x, 0) = 0$. For longitudinal stripes, the flow is also two dimensional: $\mathbf{u} = (u(y, z), v(y, z), 0)$, $u(0, z) = b(z)u_y(0, z)$, and $v(0, z) = 0$. As the problem is linear in \mathbf{u} , we seek a solution of the form

$$\mathbf{u} = \mathbf{u}_0 + \mathbf{u}_1, \quad (22)$$

where \mathbf{u}_0 is the velocity of the usual no-slip parabolic Poiseuille flow,

$$\mathbf{u}_0 = (u_0, 0, 0), \quad u_0 = -\frac{\sigma}{2\eta} y^2 + \frac{\sigma H}{2\eta} y, \quad (23)$$

and \mathbf{u}_1 is the SH slip-driven superimposed flow.

A. Longitudinal stripes

In this situation the problem is homogeneous in the x direction ($\partial/\partial x = 0$). The slip length $b(x, z) = b(z)$ is periodic in z with period L . The elementary cell is determined

as $b(z) = b$ at $|z| \leq \delta/2$, and $b(z) = 0$ at $\delta/2 < |z| \leq L/2$. In this case the velocity $\mathbf{u}_1 = (u_1, 0, 0)$ has only one nonzero component, which can be determined by solving the Laplace equation

$$\nabla^2 u_1(y, z) = 0, \quad (24)$$

with the following boundary conditions defined in the usual way as

$$u_1(H, z) = 0, \quad (25)$$

$$u_1(0, z) = b(z) \left(\frac{\sigma H}{2\eta} + \frac{\partial u_1}{\partial y} \Big|_{y=0} \right). \quad (26)$$

The Fourier method yields a general solution to this problem:

$$u_1(y, z) = (M_0 y + P_0) + \sum_{n=1}^{\infty} (M_n e^{\lambda_n y} + P_n e^{-\lambda_n y}) \cos(\lambda_n z), \quad (27)$$

with $\lambda_n = 2\pi n/L$. The sine terms vanish due to symmetry. Condition (25) leads to

$$u_1(y, z) = P_0 \left(1 - \frac{y}{H} \right) + \sum_{n=1}^{\infty} P_n \cos(\lambda_n z) e^{-\lambda_n y} \times (1 - e^{-2\lambda_n(H-y)}). \quad (28)$$

Applying the boundary condition (26) we then obtain a trigonometric dual series:

$$a_0 \left(1 + \frac{b}{H} \right) + \sum_{n=1}^{\infty} a_n [1 + b\lambda_n \coth(\lambda_n H)] \cos(\lambda_n z) = b \frac{\sigma H}{2\eta}, \quad 0 < z \leq \delta/2, \quad (29)$$

$$a_0 + \sum_{n=1}^{\infty} a_n \cos(\lambda_n z) = 0, \quad \delta/2 < z \leq L/2, \quad (30)$$

where

$$a_0 = P_0; \quad a_n = P_n(1 - e^{-2\lambda_n H}), \quad n \geq 1.$$

Dual series (29), (30) provide a complete description of hydrodynamic flow and effective slip in the longitudinal direction, given all the stated assumptions. These equations can be solved numerically (see the Appendix), but exact results are possible in the limits of thin and thick channels.

For a thin channel, $H \ll L$, we can use that $\coth t|_{t \rightarrow 0} = t^{-1} + O(t)$. By substituting this expression into Eq. (29) and keeping only values of the first nonvanishing order [53], we find

$$a_0 = \frac{2}{L} \int_0^{\delta/2} \frac{\sigma H}{2\eta} \frac{b}{1 + b/H} dz = \frac{\sigma H}{2\eta} \frac{bH\phi_2}{H + b}, \quad (31)$$

whence [21]

$$b_{\text{eff}}^{\parallel}|_{H \rightarrow 0} = \frac{bH\phi_2}{H + b\phi_1}. \quad (32)$$

This is an *exact* solution, representing a rigorous upper Wiener bound on the effective slip over all possible two-phase patterns in a thin channel. In order to gain a simple physical understanding of this result and to facilitate the analysis below,

it is instructive to mention the two limits [5,23] that follow from Eq. (32). When $H \ll b, L$ we deduce

$$b_{\text{eff}}^{\parallel}|_{H \ll b, L} \simeq \frac{\phi_2}{\phi_1} H \propto H, \quad (33)$$

and when $b \ll H \ll L$ we get a surface-averaged slip

$$b_{\text{eff}}^{\parallel}|_{b \ll H \ll L} \simeq b\phi_2 \propto b. \quad (34)$$

In the limit of a thick channel, $H \gg L$, we can use that $\coth(t \rightarrow \infty) \rightarrow 1$ and the dual series (29), (30) can be solved exactly to obtain [5]

$$b_{\text{eff}}^{\parallel} \simeq \frac{L}{\pi} \frac{\ln \left[\sec \left(\frac{\pi\phi_2}{2} \right) \right]}{1 + \frac{L}{\pi b} \ln \left[\sec \left(\frac{\pi\phi_2}{2} \right) + \tan \left(\frac{\pi\phi_2}{2} \right) \right]}. \quad (35)$$

This expression for an effective slip length depends strongly on a texture period L . When $b \ll L$ we again derive the area-averaged slip length

$$b_{\text{eff}}^{\parallel}|_{b \ll L \ll H} \simeq b\phi_2 \propto b. \quad (36)$$

When $b \gg L$, expression (35) takes the form

$$b_{\text{eff}}^{\parallel}|_{L \ll b, H} \simeq \frac{L}{\pi} \ln \left[\sec \left(\frac{\pi\phi_2}{2} \right) \right] \propto L, \quad (37)$$

which coincides with an earlier result [33] obtained for a perfect slip ($b \rightarrow \infty$) case.

B. Transverse stripes

In this case it is convenient to introduce a stream function $\psi(x, y)$ and the vorticity vector $\boldsymbol{\omega}(x, y)$. The two-dimensional velocity field corresponding to the transverse configuration is represented by $\mathbf{u}(x, y) = (\partial\psi/\partial y, -\partial\psi/\partial x, 0)$, and the vorticity vector, $\boldsymbol{\omega}(x, y) = \nabla \times \mathbf{u} = (0, 0, \omega)$, has only one nonzero component, which is equal to

$$\omega = -\nabla^2 \psi. \quad (38)$$

The solution can then be presented as the sum of the base flow with homogeneous no-slip condition and its perturbation caused by the presence of stripes as

$$\psi = \Psi_0 + \psi_1, \quad \omega = \Omega_0 + \omega_1, \quad (39)$$

where Ψ_0 and Ω_0 correspond to the typical Poiseuille flow in a flat channel with no-slip walls:

$$\Psi_0 = -\frac{\sigma}{\eta} \frac{y^3}{6} + \frac{\sigma H}{\eta} \frac{y^2}{4}, \quad \Omega_0 = \frac{\sigma}{\eta} y - \frac{\sigma H}{2\eta}. \quad (40)$$

The problem for perturbations of the stream function and z component of the vorticity vector reads

$$\nabla^2 \psi_1 = -\omega_1, \quad \nabla^2 \omega_1 = 0, \quad (41)$$

which can be solved by applying boundary conditions

$$\begin{aligned} \frac{\partial \psi_1}{\partial y}(x, 0) &= b(x) \left[\frac{\sigma H}{2\eta} - \omega_1(x, 0) \right], \\ \frac{\partial \psi_1}{\partial y}(x, H) &= 0, \quad \frac{\partial \psi_1}{\partial x}(x, H) = 0, \end{aligned} \quad (42)$$

and an extra condition that reflects our definition of the stream function:

$$\psi_1(x, 0) = 0. \quad (43)$$

This can be solved to get

$$\begin{aligned} \psi_1(x, y) &= -\frac{M_0}{4}y^2 + P_0y + \sum_{n=1}^{\infty} \left(P_n^{(1)} - \frac{M_n^{(1)}}{2} \frac{y}{\lambda_n} \right) e^{\lambda_n y} \cos \lambda_n x \\ &+ \sum_{n=1}^{\infty} \left(P_n^{(2)} + \frac{M_n^{(2)}}{2} \frac{y}{\lambda_n} \right) e^{-\lambda_n y} \cos \lambda_n x, \end{aligned} \quad (44)$$

$$\omega_1(x, y) = \frac{M_0}{2} + \sum_{n=1}^{\infty} (M_n^{(1)} e^{\lambda_n y} + M_n^{(2)} e^{-\lambda_n y}) \cos(\lambda_n x). \quad (45)$$

Conditions (42) lead to

$$\begin{aligned} P_n^{(1)} &= -P_n^{(2)} \equiv -P_n, & M_0 &= \frac{2P_0}{H}, \\ M_n^{(1)} &= -\frac{P_n(-e^{\lambda_n H} + e^{-\lambda_n H} + 2\lambda_n H e^{\lambda_n H})}{H^2 e^{\lambda_n H}}, \\ M_n^{(2)} &= -\frac{P_n(-e^{\lambda_n H} + e^{-\lambda_n H} + 2\lambda_n H e^{-\lambda_n H})}{H^2 e^{-\lambda_n H}}, \end{aligned}$$

and we obtain another dual series problem, which is similar to Eqs. (29) and (30):

$$\begin{aligned} a_0 \left(1 + \frac{b}{H} \right) + \sum_{n=1}^{\infty} a_n [1 + 2b\lambda_n V(\lambda_n H)] \cos(\lambda_n x) \\ = b \frac{\sigma H}{2\eta}, \quad 0 < x \leq \delta/2, \end{aligned} \quad (46)$$

$$a_0 + \sum_{n=1}^{\infty} a_n \cos(\lambda_n x) = 0, \quad \delta/2 < x \leq L/2. \quad (47)$$

Here,

$$a_0 = P_0; \quad a_n = \frac{\cosh(2\lambda_n H) - 2\lambda_n^2 H^2 - 1}{\lambda_n H^2} P_n, \quad n \geq 1,$$

and

$$V(t) = \frac{\sinh(2t) - 2t}{\cosh(2t) - 2t^2 - 1}. \quad (48)$$

In the limit of a thin channel [where $V(t)|_{t \rightarrow \infty} \simeq 2t^{-1} + O(t)$], the dual series problem transforms to

$$\begin{aligned} a_0 + \left(1 + \frac{3b}{H+b} \right) \sum_{n=1}^{\infty} a_n \cos(\lambda_n x) = \frac{\sigma H}{2\eta} \frac{b}{1+b/H}, \\ 0 < x \leq \delta/2, \end{aligned} \quad (49)$$

$$a_0 + \sum_{n=1}^{\infty} a_n \cos(\lambda_n x) = 0, \quad \delta/2 < x \leq L/2, \quad (50)$$

which allows one to evaluate

$$a_0 = \frac{\sigma H}{2\eta} \frac{bH\phi_2}{H + 4b - 3\phi_2 b}. \quad (51)$$

The effective slip length is then [21]

$$b_{\text{eff}}^{\perp}|_{H \rightarrow 0} = \frac{bH\phi_2}{H + 4b\phi_1}. \quad (52)$$

This exact equation represents a rigorous lower Wiener bound on the effective slip over all possible two-phase patterns in a thin channel.

For completeness here we mention again the two limiting situations:

$$b_{\text{eff}}^{\perp}|_{H \ll b, L} \simeq \frac{1}{4} \frac{\phi_2}{\phi_1} H \propto H, \quad (53)$$

$$b_{\text{eff}}^{\perp}|_{b \ll H \ll L} \simeq b\phi_2 \propto b. \quad (54)$$

In the thick channel limit, the dual series (46) and (47) take the same form as in prior work [5] [due to $V(x \rightarrow \infty) \rightarrow 1$], whence we derive [5]

$$b_{\text{eff}}^{\perp} \simeq \frac{L}{2\pi} \frac{\ln \left[\sec \left(\frac{\pi\phi_2}{2} \right) \right]}{1 + \frac{L}{2\pi b} \ln \left[\sec \left(\frac{\pi\phi_2}{2} \right) + \tan \left(\frac{\pi\phi_2}{2} \right) \right]}. \quad (55)$$

The consideration as above of the same limits of small and large b give

$$b_{\text{eff}}^{\perp}|_{b \ll L \ll H} \simeq b\phi_2 \propto b \quad (56)$$

and

$$b_{\text{eff}}^{\perp}|_{L \ll b, H} \simeq \frac{L}{2\pi} \ln \left[\sec \left(\frac{\pi\phi_2}{2} \right) \right] \propto L. \quad (57)$$

C. Tilted stripes

If the stripes are inclined at an angle Θ , the effective slip length of the channel, $b_{\text{eff}}^{(x)}$, can be calculated with Eq. (21), provided that effective slip in eigendirections is determined from the numerical solution of Eqs. (29), (30) and (46), (47). Some simple analytical results are possible in the limit of thin and thick channels.

In the case of a thin channel and large local slip, $H \ll \min\{b, L\}$, substitution of Eqs. (33) and (53) into Eq. (21) gives

$$b_{\text{eff}}^{(x)} \simeq \frac{H\phi_2}{4\phi_1} \frac{4\phi_2 + \phi_1 + 3\phi_1 \cos^2 \Theta}{4\phi_2 + \phi_1 - 3\phi_2 \cos^2 \Theta}. \quad (58)$$

Interestingly, in this limit $b_{\text{eff}}^{(x)}$ does not depend on b , being a function of only H and a fraction of the gas area. At small b according to Eqs. (34) and (54), $b_{\text{eff}}^{\parallel} \simeq b_{\text{eff}}^{\perp} \simeq b_{\text{eff}}^{(x)}$, so that the flow becomes isotropic.

In the limit of a thick channel and sufficiently large local slip, we can simplify Eq. (21) and define the downstream effective slip length as

$$b_{\text{eff}}^{(x)} \simeq (b_{\text{eff}}^{\parallel} - b_{\text{eff}}^{\perp}) \cos^2 \Theta + b_{\text{eff}}^{\perp}, \quad (59)$$

with $b_{\text{eff}}^{\parallel,\perp}$ given by Eqs. (35) and (55). In the limit of perfect local slip it can be further simplified to get

$$b_{\text{eff}}^{(x)} \simeq b_{\text{eff}}^{\perp} (1 + \cos^2 \Theta). \quad (60)$$

Using Eqs. (36) and (56) we conclude that the flow is isotropic, $b_{\text{eff}}^{\parallel} \simeq b_{\text{eff}}^{\perp} \simeq b_{\text{eff}}^{(x)}$, when b is much smaller than the texture period.

V. SIMULATION METHOD

To simulate fluid flow between parallel patterned plates a number of simulation methods could be used. These include molecular dynamics, dissipative particle dynamics, stochastic rotation dynamics, classical finite element or finite volume solvers, as well as the LB method. Since the current paper does not address molecular interactions or liquid-gas transitions close to the surface, one can limit the required computational effort by applying a continuum solver for the Stokes equation together with appropriate boundary conditions to model local slip. As detailed further below, in particular, in the thin channel limit with $H \ll \min\{b, L\}$ a very high resolution of the flow field is needed in order to measure b_{eff} with required precision. Thus, simulation methods which require time averaging of the flow field or finite length scales to resolve a slip boundary render less efficient for the current problem. While finite element or finite volume solvers would be suitable alternatives, we apply the LB method [37].

The LB approach is based on the Boltzmann kinetic equation

$$\left[\frac{\partial}{\partial t} + \mathbf{u} \cdot \nabla_{\mathbf{r}} \right] f(\mathbf{r}, \mathbf{u}, t) = \Omega, \quad (61)$$

which describes the evolution of the single particle probability density $f(\mathbf{r}, \mathbf{u}, t)$, where \mathbf{r} is the position, \mathbf{u} is the velocity, and t is the time. The derivatives on the left-hand side represent propagation of particles in phase space, whereas the collision operator Ω takes into account molecular collisions.

In the LB method the time t , the position \mathbf{r} , and the velocity \mathbf{u} are discretized. In units of the lattice constant Δx and the time step Δt this leads to a discretized version of Eq. (61):

$$f_k(\mathbf{r} + \mathbf{c}_k, t + 1) - f_k(\mathbf{r}, t) = \Omega_k, \quad k = 0, 1, \dots, B. \quad (62)$$

Our simulations are performed on a three-dimensional lattice with $B = 19$ discrete velocities (the so-called D3Q19 model). With a proper choice of the discretized collision operator Ω it can be shown that the flow behavior follows the Navier-Stokes equation [37]. We choose the Bhatnagar-Gross-Krook (BGK) form [38]

$$\Omega_k = -\frac{1}{\tau} [f_k(\mathbf{r}, t) - f_k^{\text{eq}}(\mathbf{u}(\mathbf{r}, t), \rho(\mathbf{r}, t))], \quad (63)$$

which assumes a relaxation toward a discretized local Maxwell-Boltzmann distribution f_k^{eq} . Here, τ is the mean collision time that determines the kinematic viscosity $\nu = \frac{2\tau-1}{6}$ of the fluid. In this study it is kept constant at $\tau = 1.0$.

Physical properties of the simulated fluid are given by the stochastic moments of the distribution function. Of special interest are the conserved quantities, namely, the fluid density $\rho(\mathbf{r}, t) = \rho_0 \sum_k f_k(\mathbf{r}, t)$ and the momentum $\rho(\mathbf{r}, t) \mathbf{u}(\mathbf{r}, t) = \rho_0 \sum_k c_k f_k(\mathbf{r}, t)$, with ρ_0 being a reference density.

Within the LB method a common approach to describe the interaction between hydrophobic surfaces and the fluid is by means of a repulsive force term [14,15,39–41]. This force applied at the boundary can be linked to the contact angle to quantitatively describe the wettability of materials [15,42–44]. Alternatively, slip can be introduced by generalizing the no-slip bounce-back boundary conditions in order to allow specular reflections with a given probability [45–47], or to apply diffuse scattering [48–50]. The method we apply here follows the latter idea and uses a second order accurate on-site fixed velocity boundary condition to simulate wall slippage. The on-site velocity boundary condition is used to set a required slip length on the patterned surface. For the details of the implementation we refer the reader to [51,52].

Our geometry of configuration is the same as sketched in Fig. 1, but in simulations we employ periodic boundary conditions in the x and z directions, which allows one to reduce the simulation domain to a pseudo-two-dimensional (2D) system. To drive the flow a constant pressure gradient is applied in the x direction by means of a homogeneous acceleration, g , in the whole fluid domain. Even though the simulation domain can be reduced to be pseudo-2D, we find that the simulation of fluid flow with a large slip in the thin channel limit still requires a system of several million cells in order to properly resolve the velocity field. The key issue is, here, that in order to resolve large slip lengths a minimum channel height is necessary. To reach the thin channel limit the stripe length has to be increased to even larger values.

Following the definition given for the Fourier analysis in Sec. IV, all heights H and slip lengths b are given nondimensionalized for a stripe length of $L = 2\pi$. The resolution of the simulated system is then given by the lattice constant

$$\Delta x = \frac{HL}{2\pi\mathcal{N}}, \quad (64)$$

where \mathcal{N} is the number of discretization points used to resolve the height of the channel. While systems with a height of $H = 1.0$ can be simulated using a discretization of $1 \times 32 \times 200\Delta x^3$ only, decreasing H to 0.1 causes the required system size to be $1 \times 70 \times 4400\Delta x^3$. To successfully recover the exact results in the thin channel limit ($H = 0.01$) a system of size $1 \times 104 \times 64000\Delta x^3$ has to be simulated.

The number of time steps required to reach a steady state depends on the channel height, the velocity of the flow as determined by the driving acceleration, as well as the fraction of slip and no-slip area at the surface. For the simulations conducted in the thin channel limit a steady state velocity field exactly fitting the theoretical prediction develops after one to four million timesteps. In the thick channel limit, however, the number of timesteps required can be an order of magnitude larger limiting the maximum feasible system height. Moreover, the transition between slip and no-slip stripes induces a distortion of the flow field with a range of $\simeq 3\Delta x$. In order to keep the induced error below an acceptable limit, a minimum resolution of the channel length of $64\Delta x$ is maintained. Additionally, the maximum flow velocity is limited due to the low Mach number assumption of our lattice Boltzmann implementation. In effect, the acceleration modeling the pressure gradient has to be reduced increasing the time required for convergence. For example, a simulation

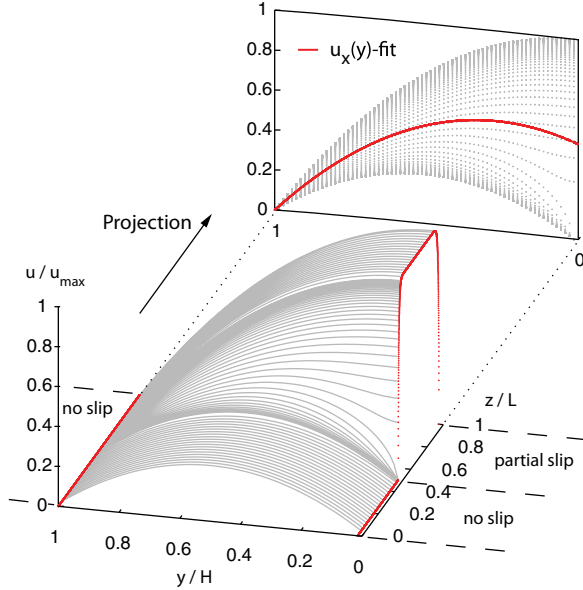


FIG. 2. (Color online) Illustration of the measurement of effective slip eigenvalues from lattice Boltzmann simulations. The velocity information of the whole domain is projected onto a single plane. To this cloud of data, Eq. (65) is fitted, effectively averaging the flow field over the whole channel.

domain of $1 \times 1024 \times 64\Delta x^3$ as used to model the thick channel limit at $H \simeq 100$ requires 12.5×10^6 time steps to equilibrate.

We compare measurements of b_{eff} by permeability estimates and velocity profiles, respectively. The permeability is calculated from measurements of the flow rate, according to Eq. (14). This allows one to determine the effective slip by Eq. (19). Alternatively, the profiles of the velocity in flow direction are averaged over the whole system by projecting the velocity information of the whole domain onto a single plane. Then, the effective slip length b_{eff} is found by a Levenberg-Marquardt fit of the adjusted Hagen-Poiseuille equation

$$u_x(y) = \frac{gH^2}{2\eta} \left(\frac{(y-H)^2}{H^2} - \frac{(y-H) + b_{\text{eff}}}{(H + b_{\text{eff}})} \right), \quad (65)$$

with the known g and H (see Fig. 2 for an illustration).

The error of the effective slip measurements is determined by two factors, namely, the resolution of the channel height and the absolute slip length of the partially slipping stripes. For poorly resolved channels with $10 < \mathcal{N} < 30$ and small slip lengths the permeability measurements still produce accurate results, whereas a fit of the velocity profiles fails. If $b \gg H$, however, the quality of the obtained data declines. For an increase in resolution ($30 < \mathcal{N} \leq 100$) both approaches allow very precise measurements for intermediate slip lengths of up to two orders of magnitude larger than the channel height. However, if b is increased further, due to discretization the error in the effective slip determined by the permeability measurement increases significantly, rendering this method inefficient since a higher resolution would be required. For example, to keep the error in the determination of a prescribed slip in the order of $10^5 \Delta x$ below 5% the permeability method

requires the channel height to be resolved by 200 lattice sites, while for the measurement by fitting the velocity profiles 100 sites suffice.

To validate the concept of a tensorial slip by simulations of a flow past tilted stripes, we do not rotate the surface pattern with respect to the lattice, but instead change the direction of the acceleration in the y - z plane. This avoids discretization errors due to the underlying regular lattice occurring in case of a rotated surface pattern. We extract the downstream slip by projecting the slip measured on the main axes onto the pressure gradient direction.

VI. RESULTS AND DISCUSSION

In this section we compare results of our LB simulation with analytical example calculations and numerical solutions of the dual series (29), (30) and (46), (47) (see the Appendix).

As a benchmark for the simulation, we start with a thin channel, where striped surfaces were shown to provide rigorous upper and lower Wiener bounds on the effective slip over all possible two-phase patterns [21]. In order to reach the thin channel limit, a dimensionless height of $H = 0.01$ is chosen. The slip lengths are set to $b = 10^{-3}H$ ($0.1\Delta x$) and $b = 10^3H$ ($102\,000\Delta x$), each differing three orders of magnitude from the channel height and reaching the limits of small [cf. Eqs. (34) and (54)] as well as large slip Eqs. (33) and (53). As preparatory tests showed, a minimum channel height of $H = 100\Delta x$ is required to measure slip lengths of $b = 10^3H$ corresponding to $10^5\Delta x$. For a dimensionless height of $H = 0.01$, we choose a simulation domain of $1 \times 104 \times 64\,000\Delta x^3$. For each of the two slip lengths, longitudinal and transverse flow was simulated for a different fraction of surface gas phase, ranging from no slip ($\phi_2 = 0$) to homogeneous partial slip ($\phi_2 = 1$). The local acceleration here (and below for thin channel simulations) was kept at $g = 10^{-6}\Delta x/\Delta t^2$.

Figure 3 shows the exact eigenvalues of the effective slip tensor in the thin channel limit, Eqs. (32), (52), for both slip lengths b . The fit of the simulation data and the analytical limits is excellent for all separations. In the case of small local slip in the thin channel the effective slip remains isotropic despite the inhomogeneity of the boundary. For large local slip, we observe truly tensorial effective slip and highly anisotropic flow over the surface. These simulations demonstrate that finite size effects and resolution effects are well controlled, and the size of the system is sufficient to avoid artifacts. Another important point to note is that in our theoretical analysis all equations were derived ignoring stripe edge effects. An excellent agreement between theoretical and simulation results indicates that the edge effects do not influence the simulation results significantly.

Figure 4 shows the eigenvalues of the effective slip-length tensor as a function of ϕ_2 for a thick gap. For these simulations the acceleration has been reduced down to $g = 10^{-7}\Delta x/\Delta t^2$ to obey the low Mach number (see Sec. V) limit. The time to reach a stable state increased then to $15 \times 10^6\Delta t$. Simulation results are presented for two different slip lengths of $b = 1.0$ and $b = 10.0$ in a system of $H = 0.1$, where L is now resolved by 4400 lattice sites. The theoretical solutions represented by the lines were obtained by the dual series approach. We find

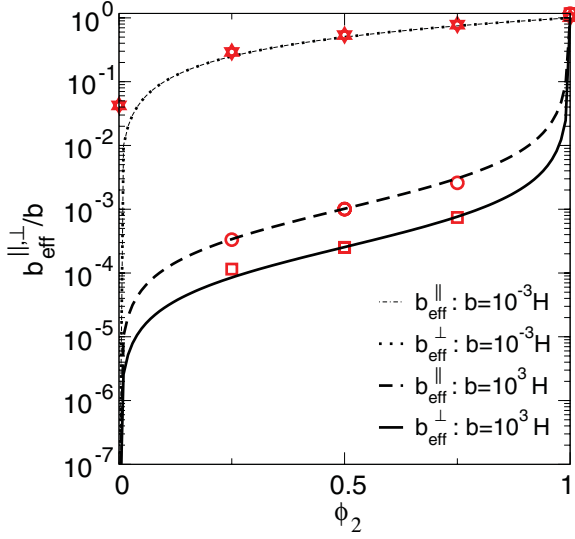


FIG. 3. (Color online) Eigenvalues of the effective slip-length tensors simulated in the limit of a thin channel (symbols). The lines represent results of theoretical calculations by Eqs. (32) and (52). The data show that at small b the eigenvalues of \mathbf{b}_{eff} decrease as compared to a large local slip at the gas sector, and that the slip-length tensor becomes isotropic resulting in $b_{\text{eff}}^{\perp,||}$ to become hardly distinguishable in the $b = 10^{-3}H$ case.

that the fit is excellent for all fractions of the slipping area, indicating that our semianalytical theory is extremely accurate. The data presented in Fig. 4 show larger effective slip for a lower slip to height ratio, i.e., a thicker channel. This illustrates well the earlier suggestion that effective boundary conditions for this channel geometry are controlled by the smallest length scale of the problem [23].

To check the validity of the tensorial slip approach, we now orient the texture relative to the x axis, which in our

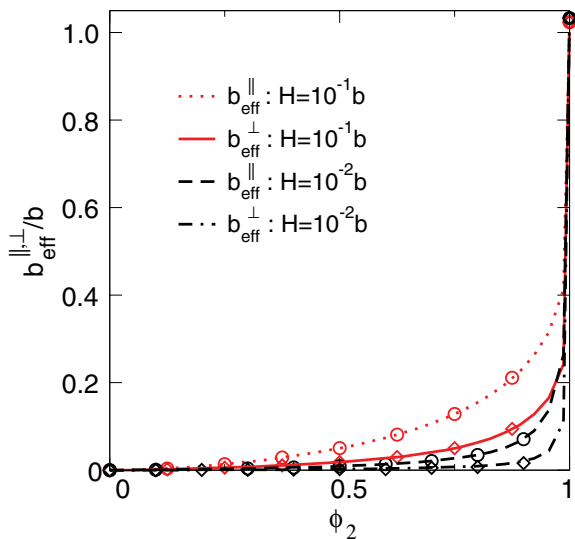


FIG. 4. (Color online) Simulation results of eigenvalues of \mathbf{b}_{eff} as a function of fraction of gas sectors, ϕ_2 , in the limit of a thick channel (symbols). Lines represent corresponding theoretical values obtained by a numerical solution of Eqs. (29), (30) and (46), (47).

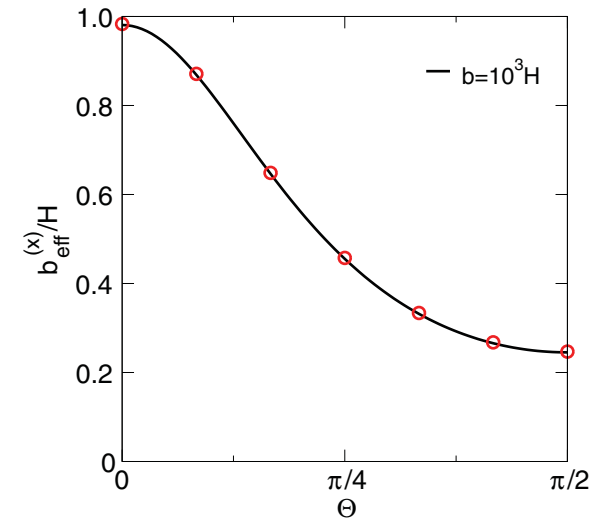
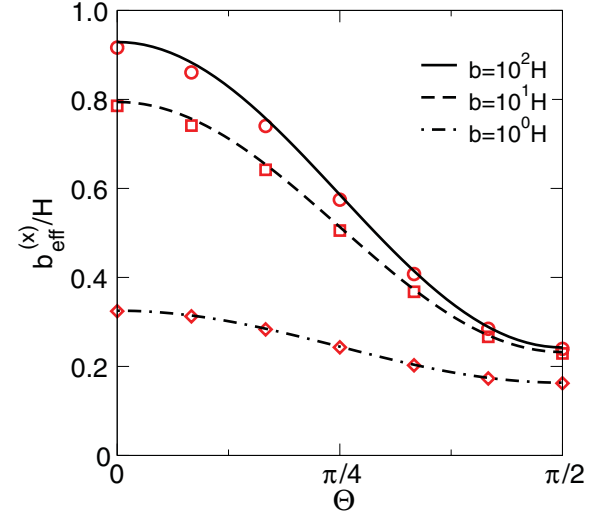


FIG. 5. (Color online) Downstream effective slip lengths of the thin channel simulated at $\phi_2 = 0.5$ for stripes inclined at different angle Θ (symbols). Especially in the limiting case (b) the value of $b_{\text{eff}}^{(x)}$ has to be calculated from the measured eigenvalues by Eq. (21). All the lines are predicted theoretically downstream slip lengths: (a) calculated by using Eq. (1) [or Eq. (21)] with eigenvalues of \mathbf{b}_{eff} determined from numerical solutions of (29), (30) and (46), (47); (b) calculated with Eq. (58).

model is always aligned with the applied pressure gradient. Figures 5 and 6 show two sets of effective downstream slip lengths simulated with several Θ , but fixed $H = 0.1$ and $\phi_2 = 0.5$, which results in a maximum transverse flow in a thin channel situation [22].

In the first set (Fig. 5), we consider thin channels and vary b/H from 1 to 1000. Figure 5(a) shows simulation data obtained using a channel of height $H = 0.1$. Further, theoretical curves calculated with Eq. (1) are presented. Here, eigenvalues of the slip-length tensor are obtained by numerical solution of the dual series. The fits of the simulation data are in very good agreement with the numerical solutions of the dual series suggesting the validity of the concept of a tensorial slip in a thin channel situation. Note that the simulation

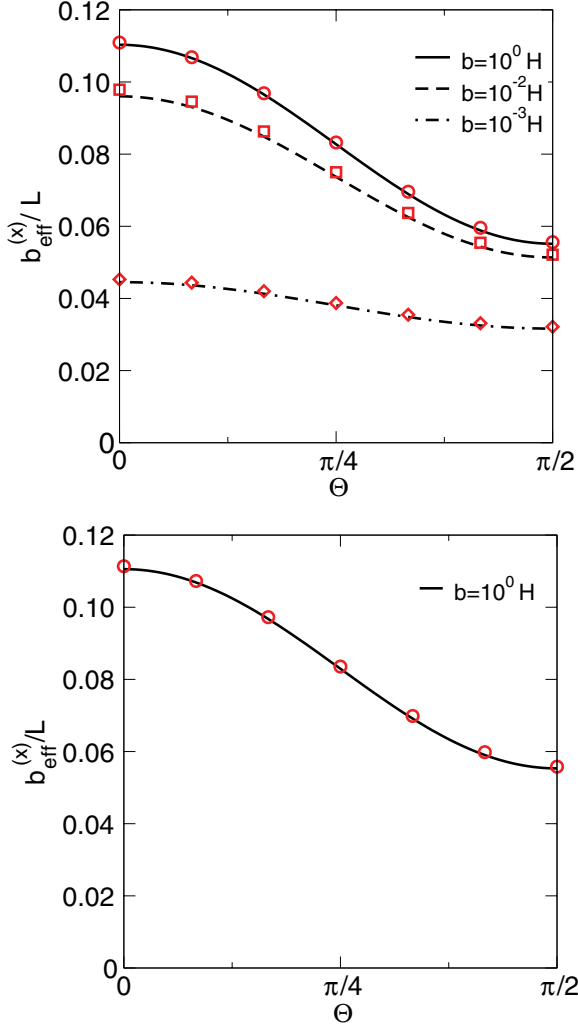


FIG. 6. (Color online) Effective downstream slip lengths for tilted stripes (the thick channel limit) simulated at $\phi_2 = 0.5$ (symbols). All the lines are predicted theoretically downstream slip lengths: (a) calculated by using Eq. (1) [or Eq. (21)] with eigenvalues of \mathbf{b}_{eff} determined from numerical solutions of Eqs. (29), (30) and (46), (47); (b) calculated with Eq. (59) with eigenvalues evaluated with Eqs. (37) and (57).

results of Fig. 5(a) cannot be compared with the analytical expression, Eq. (58), because Fig. 5(a) is based on a relatively moderate value of local slip at the gas sectors, whereas Eq. (58) requires very large b . To validate predictions of this analytical formula, the channel height was decreased down to $H = 0.01$. Simulation results are presented in Fig. 5(b), confirming the surprising accuracy of a simple analytical expression, Eq. (58). We remark that in this important limit of validity of Eq. (58), $b_{\text{eff}}^{(x)}/H$ is quite large, although $b_{\text{eff}}^{(x)}$ itself is small. This may have implications for a reduction of a hydrodynamic drag force [23,24]. Passive mixing might also be an interesting application, since the anisotropy of flow is very large, which is optimal for a transverse flow generation [22]. We suggest that our simple asymptotic result could be intensively used to simplify theoretical analysis of these important phenomena.

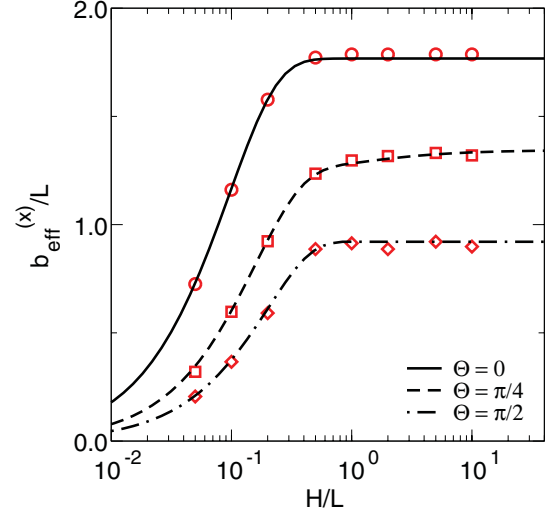


FIG. 7. (Color online) Effective downstream slip lengths at different channel thickness ($\phi_2 = 0.75$, $b/L = 5.0$). Symbols illustrate the simulation data, and curves show theoretical predictions.

In the second set as shown in Fig. 6 a thick channel (of height $H = 100$) is simulated. Figure 6(a) plots simulation results for several b/H varying from 10^{-3} to 1 (symbols). Similarly to previous examples, we found very good agreement between simulation results and predictions of tensorial Eq. (1) with eigenvalues computed with our semianalytical theory. We found that already for the case $b = H = 100$ our simulations reach the limit of large slip in the thick channel, so that the comparison with analytical solutions is possible. To examine this more closely, the simulation results obtained in this limit are reproduced in Fig. 6(b). Also included are the theoretical results calculated with asymptotic formulas, Eqs. (37) and (57), which perfectly fit simulation data.

Finally, we simulate the downstream slip length as a function of the channel thickness with the focus on the intermediate gap situation. Figure 7 shows the typical simulation results (the example corresponds to $b/L = 5.0$ and $\phi_2 = 0.75$) and demonstrates that the effective slip lengths increase with H and saturate for a thick gap. This fully confirms the statement that an effective boundary condition is not a characteristic of the liquid-solid interface alone, but depends on the flow configuration and interplay between the typical length scales of the problem. Again, the simulation and theoretical data are in excellent agreement for longitudinal, transverse, and tilted stripes. Thus, Fig. 7 unambiguously shows that the tensorial slip boundary condition, originally justified for a thick channel, to any channel thickness can be generalized to any channel thickness.

VII. CONCLUSION

We have investigated pressure-driven flow in a flat-parallel channel with one hydrophilic and one superhydrophobic surface, and have given some general theoretical arguments showing that a concept of an effective tensorial slip is valid for any thickness (compared to a superhydrophobic texture scale). The eigenvalues of the effective slip-length tensor

depend on the gap, so that they cannot be viewed as a local property of the superhydrophobic surface, except in the thick channel limit. Instead, the slip-length tensor represents a global characteristic of the channel. The mathematical properties of the slip-length and permeability tensors allowed us to derive a simple analytical formula for an effective downstream slip length in the case of inclined to a pressure gradient textures. Our analysis is validated by means of LB simulations.

ACKNOWLEDGMENTS

We have benefited from discussions with M. Z. Bazant at the initial stage of this study. This research was partly supported by the Russian Academy of Science (RAS) through its priority program ‘‘Assembly and Investigation of Macromolecular Structures of New Generations,’’ by the Netherlands Organization for Scientific Research (NWO/STW VIDI), and by the German Science Foundation (DFG) through its priority program ‘‘Micro- and nanofluidics’’ and the collaborative research center (SFB) 716. We acknowledge computing resources from the J ulich Supercomputing Center and the Scientific Supercomputing Center Karlsruhe.

APPENDIX: NUMERICAL METHOD

Equations (29), (30) and (46), (47) provide a complete description of hydrodynamic flow and effective slip in eigendirections. Their exact solution is possible for the limits of a thin and a thick channel only. In order to solve the problem for general channel thickness, the following numerical algorithm has been used.

It is convenient to change to dimensionless values. We, therefore, choose $L/(2\pi)$ as the reference length scale and $\sigma HL/(4\pi\eta)$ as the velocity scale. We make the substitution

$$(x, y, z) = \frac{L}{2\pi}(\tilde{x}, \tilde{y}, \tilde{z}), \quad H = \frac{L}{2\pi}\tilde{H}, \quad b = \frac{L}{2\pi}\tilde{b}, \quad (\text{A1})$$

$$a_n = \frac{\sigma HL}{4\pi\eta}\tilde{a}_n, \quad n \geq 0, \quad (\text{A2})$$

where nondimensional variables are denoted by tildes. This procedure gives the dual series problem for longitudinal flow in the form

$$\tilde{a}_0 \left(1 + \frac{\tilde{b}}{\tilde{H}}\right) + \sum_{n=1}^{\infty} \tilde{a}_n [1 + \tilde{b}n \coth(n\tilde{H})] \cos(n\tilde{z}) = \tilde{b}, \quad 0 < \tilde{z} \leq c, \quad (\text{A3})$$

$$\tilde{a}_0 + \sum_{n=1}^{\infty} \tilde{a}_n \cos(n\tilde{z}) = 0, \quad c < \tilde{z} \leq \pi, \quad (\text{A4})$$

where $c = \pi\phi_2 = \pi\delta/L$. Similarly, the equations for the flow in the direction orthogonal to the stripes is written as

$$\tilde{a}_0 \left(1 + \frac{\tilde{b}}{\tilde{H}}\right) + \sum_{n=1}^{\infty} \tilde{a}_n [1 + 2\tilde{b}nV(n\tilde{H})] \cos(n\tilde{x}) = \tilde{b}, \quad 0 < \tilde{x} \leq c, \quad (\text{A5})$$

$$\tilde{a}_0 + \sum_{n=1}^{\infty} \tilde{a}_n \cos(n\tilde{x}) = 0, \quad c < \tilde{x} \leq \pi. \quad (\text{A6})$$

After integrating Eq. (A3) over $[0, \tilde{z}]$ and Eq. (A5) over $[0, \tilde{x}]$, we multiply the result by $\sin(m\tilde{z})$ [$\sin(m\tilde{x})$, respectively], where m is a non-negative integer. We then integrate again over $[0, c]$. Equation (A4) is multiplied by $\cos(m\tilde{z})$ and Eq. (A6) by $\cos(m\tilde{x})$ and we then integrate over $[c, \pi]$. The resulting equations are summarized to obtain a system of linear algebraic equations,

$$\sum_{n=0}^{\infty} A_{nm} \tilde{a}_n = B_m, \quad (\text{A7})$$

which can be solved with respect to \tilde{a}_n by standard numerical algebra tools.

The coefficients for the longitudinal case are ($m \geq 0$)

$$A_{0m}^{\parallel} = \left(1 + \frac{\tilde{b}}{\tilde{H}}\right) \int_0^c \tilde{z} \sin(m\tilde{z}) d\tilde{z} + \int_c^{\pi} \cos(m\tilde{z}) d\tilde{z}, \quad (\text{A8})$$

$$A_{nm}^{\parallel} = \frac{1 + \tilde{b}n \coth(n\tilde{H})}{n} \int_0^c \sin(m\tilde{z}) \sin(n\tilde{z}) d\tilde{z} + \int_c^{\pi} \cos(m\tilde{z}) \cos(n\tilde{z}) d\tilde{z}, \quad n \geq 1, \quad (\text{A9})$$

$$B_m^{\parallel} = \tilde{b} \int_0^c \tilde{z} \sin(m\tilde{z}) d\tilde{z}. \quad (\text{A10})$$

For transverse flow we get

$$A_{nm}^{\perp} = \frac{1 + 2\tilde{b}nV(n\tilde{H})}{n} \int_0^c \sin(m\tilde{z}) \sin(n\tilde{z}) d\tilde{z} + \int_c^{\pi} \cos(m\tilde{z}) \cos(n\tilde{z}) d\tilde{z}, \quad n \geq 1, \quad (\text{A11})$$

$$A_{0m}^{\perp} = A_{0m}^{\parallel}, \quad B_m^{\perp} = B_m^{\parallel}. \quad (\text{A12})$$

For the numerical evaluation, the linear system is truncated and reduced to a $N \times N$ matrix and the solution is then found to converge upon truncation refinement. According to the definition

$$b_{\text{eff}} = \frac{\langle u_s \rangle}{\left(\left(\frac{\partial u}{\partial y}\right)_s\right)}, \quad (\text{A13})$$

the dimensionless and dimensional effective slip lengths are given by

$$\tilde{b}_{\text{eff}} = \frac{\tilde{a}_0}{1 - \tilde{a}_0/\tilde{H}}, \quad (\text{A14})$$

$$b_{\text{eff}} = \frac{L}{2\pi} \tilde{b}_{\text{eff}}. \quad (\text{A15})$$

[1] H. A. Stone, A. D. Stroock, and A. Ajdari, *Annu. Rev. Fluid Mech.* **36**, 381 (2004).

[2] T. M. Squires and S. R. Quake, *Rev. Mod. Phys.* **77**, 977 (2005).

[3] O. I. Vinogradova, *Int. J. Min. Process.* **56**, 31 (1999).

[4] E. Lauga, M. P. Brenner, and H. A. Stone, in *Handbook of Experimental Fluid Dynamics*, Chap. 19 (Springer, NY, 2007), pp. 1219–1240.

[5] O. I. Vinogradova and A. V. Belyaev, *J. Phys.: Condens. Matter* **23**, 184104 (2011).

[6] K. Kamrin, M. Bazant, and H. A. Stone, *J. Fluid Mech.* **658**, 409 (2010).

[7] D. Quere, *Rep. Prog. Phys.* **68**, 2495 (2005).

[8] C. H. Choi, U. Ulmanella, J. Kim, C. M. Ho, and C. J. Kim, *Phys. Fluids* **18**, 087105 (2006).

[9] P. Joseph, C. Cottin-Bizonne, J. M. Benoît, C. Ybert, C. Journet, P. Tabeling, and L. Bocquet, *Phys. Rev. Lett.* **97**, 156104 (2006).

[10] P. Tsai, A. M. Peters, C. Pirat, M. Wessling, R. G. H. Lammerting, and D. Lohse, *Phys. Fluids* **21**, 112002 (2009).

[11] J. P. Rothstein, *Annu. Rev. Fluid Mech.* **42**, 89 (2010).

[12] O. I. Vinogradova, K. Koynov, A. Best, and F. Feuillebois, *Phys. Rev. Lett.* **102**, 118302 (2009).

[13] O. I. Vinogradova and G. E. Yakubov, *Langmuir* **19**, 1227 (2003).

[14] J. Hyväluoma and J. Harting, *Phys. Rev. Lett.* **100**, 246001 (2008).

[15] J. Harting, C. Kunert, and H. Herrmann, *Europhys. Lett.* **75**, 328 (2006).

[16] C. Cottin-Bizonne, B. Cross, A. Steinberger, and E. Charlaix, *Phys. Rev. Lett.* **94**, 056102 (2005).

[17] L. Joly, C. Ybert, and L. Bocquet, *Phys. Rev. Lett.* **96**, 046101 (2006).

[18] C. Ybert, C. Barentin, C. Cottin-Bizonne, P. Joseph, and L. Bocquet, *Phys. Fluids* **19**, 123601 (2007).

[19] M. Z. Bazant and O. I. Vinogradova, *J. Fluid Mech.* **613**, 125 (2008).

[20] L. Bocquet and J. L. Barrat, *Soft Matter* **3**, 685 (2007).

[21] F. Feuillebois, M. Z. Bazant, and O. I. Vinogradova, *Phys. Rev. Lett.* **102**, 026001 (2009).

[22] F. Feuillebois, M. Z. Bazant, and O. I. Vinogradova, *Phys. Rev. E* **82**, 055301(R) (2010).

[23] A. V. Belyaev and O. I. Vinogradova, *Soft Matter* **6**, 4563 (2010).

[24] E. S. Asmolov, A. V. Belyaev, and O. I. Vinogradova, *Phys. Rev. E* **84**, 026330 (2011).

[25] D. Andrienko, P. Patricio, and O. I. Vinogradova, *J. Chem. Phys.* **121**, 4414 (2004).

[26] G. E. Yakubov, H. J. Butt, and O. I. Vinogradova, *J. Phys. Chem. B* **104**, 3407 (2000).

[27] J. W. G. Tyrrell and P. Attard, *Phys. Rev. Lett.* **87**, 176104 (2001).

[28] N. V. Priezjev, A. A. Darhuber, and S. M. Troian, *Phys. Rev. E* **71**, 041608 (2005).

[29] A. M. J. Davis and E. Lauga, *Phys. Fluids* **21**, 011701 (2009).

[30] M. Sbragaglia and A. Prosperetti, *Phys. Fluids* **19**, 043603 (2007).

[31] A. D. Stroock, S. K. Dertinger, G. M. Whitesides, and A. Ajdari, *Anal. Chem.* **74**, 5306 (2002).

[32] A. Ajdari, *Phys. Rev. E* **65**, 016301 (2001).

[33] E. Lauga and H. A. Stone, *J. Fluid Mech.* **489**, 55 (2003).

[34] A. V. Belyaev and O. I. Vinogradova, *J. Fluid Mech.* **652**, 489 (2010).

[35] S. S. Bahga, O. I. Vinogradova, and M. Z. Bazant, *J. Fluid Mech.* **644**, 245 (2010).

[36] A. V. Belyaev and O. I. Vinogradova, *Phys. Rev. Lett.* **107**, 098301 (2011).

[37] S. Succi, *The Lattice Boltzmann Equation for Fluid Dynamics and Beyond* (Oxford University Press, New York, 2001).

[38] P. L. Bhatnagar, E. P. Gross, and M. Krook, *Phys. Rev.* **94**, 511 (1954).

[39] L. Zhu, D. Trethewey, L. Petzold, and C. Meinhart, *J. Comput. Phys.* **202**, 181 (2005).

[40] R. Benzi, L. Biferale, M. Sbragaglia, S. Succi, and F. Toschi, *Europhys. Lett.* **74**, 651 (2006).

[41] J. Zhang and D. Y. Kwok, *Phys. Rev. E* **70**, 056701 (2004).

[42] R. Benzi, L. Biferale, M. Sbragaglia, S. Succi, and F. Toschi, *Phys. Rev. E* **74**, 021509 (2006).

[43] H. Huang, D. T. Thorne, M. G. Schaap, and M. C. Sukop, *Phys. Rev. E* **76**, 066701 (2007).

[44] S. Schmieschek and J. Harting, *Comm. Comp. Phys.* **9**, 1165 (2011).

[45] S. Succi, *Phys. Rev. Lett.* **89**, 064502 (2002).

[46] G. H. Tang, W. Q. Tao, and Y. L. He, *Phys. Fluids* **17**, 058101 (2005).

[47] M. Sbragaglia and S. Succi, *Phys. Fluids* **17**, 093602 (2005).

[48] S. Ansumali and I. V. Karlin, *Phys. Rev. E* **66**, 026311 (2002).

[49] V. Sofonea and R. F. Sekerka, *Phys. Rev. E* **71**, 066709 (2005).

[50] X. D. Niu, C. Shu, and Y. T. Chew, *Europhys. Lett.* **67**, 600 (2004).

[51] M. Hecht and J. Harting, *J. Stat. Mech.: Theory Exp.* (2010) P01018.

[52] N. K. Ahmed and M. Hecht, *J. Stat. Mech.: Theory Exp.* (2009) P09017.

[53] Note that a_n scale with $\sigma H/\eta$. By using an appropriate scale for coefficients a_n [see Eq. (A2)] it is easy to show that the right-hand side of the dual series does not scale with H .